



HAL
open science

Dwarf Galaxies in the MATLAS Survey: Hubble Space Telescope Observations of the Globular Cluster System in the Ultra-diffuse Galaxy MATLAS-2019

Oliver Müller, Patrick Durrell, Francine Marleau, Pierre-Alain Duc, Sungsoon Lim, Lorenzo Posti, Adriano Agnello, Rubén Sánchez-Janssen, Mélina Poulain, Rebecca Habas, et al.

► To cite this version:

Oliver Müller, Patrick Durrell, Francine Marleau, Pierre-Alain Duc, Sungsoon Lim, et al.. Dwarf Galaxies in the MATLAS Survey: Hubble Space Telescope Observations of the Globular Cluster System in the Ultra-diffuse Galaxy MATLAS-2019. *The Astrophysical Journal*, 2021, 923 (1), pp.9. 10.3847/1538-4357/ac2831 . hal-03479317

HAL Id: hal-03479317

<https://hal.science/hal-03479317v1>

Submitted on 6 Jan 2025







HAL is a multi-disciplinary open access archive for the deposit and dissemination of scientific research documents, whether they are published or not. The documents may come from teaching and research institutions in France or abroad, or from public or private research centers.

L'archive ouverte pluridisciplinaire **HAL**, est destinée au dépôt et à la diffusion de documents scientifiques de niveau recherche, publiés ou non, émanant des établissements d'enseignement et de recherche français ou étrangers, des laboratoires publics ou privés.



Distributed under a Creative Commons Attribution 4.0 International License

Dwarf galaxies in the MATLAS survey: Hubble Space Telescope observations of the globular cluster system in the ultra-diffuse galaxy MATLAS-2019

OLIVER MÜLLER ^{1,2} PATRICK R. DURRELL,³ FRANCINE R. MARLEAU ⁴ PIERRE-ALAIN DUC,¹ SUNGSOON LIM,⁵ LORENZO POSTI ¹ ADRIANO AGNELLO,⁶ RUBÉN SÁNCHEZ-JANSSEN ⁷ MÉLINA POULAIN,⁸ REBECCA HABAS ¹ ERIC EMSELLEM,^{9,10} SANJAYA PAUDEL ¹¹ REMCO F. J. VAN DER BURG,⁹ AND JÉRÉMY FENSCH¹⁰

¹*Observatoire Astronomique de Strasbourg (ObAS), Université de Strasbourg - CNRS, UMR 7550 Strasbourg, France*

²*Institute of Physics, Laboratory of Astrophysics, École Polytechnique Fédérale de Lausanne (EPFL), 1290 Sauverny, Switzerland*

³*Department of Physics, Astronomy, Geology and Environmental Sciences, Youngstown State University, Youngstown, OH 44555 USA*

⁴*Institut für Astro- und Teilchenphysik, Universität Innsbruck, Technikerstraße 25/8, Innsbruck, A-6020, Austria*

⁵*University of Tampa, 401 West Kennedy Boulevard, Tampa, FL 33606, USA*

⁶*DARK, Niels-Bohr Institute, Lyngbyvej 2, Copenhagen, Denmark*

⁷*UK Astronomy Technology Centre, Royal Observatory, Blackford Hill, Edinburgh, EH9 3HJ, UK*

⁸*Institut für Astro- und Teilchenphysik, Universität Innsbruck, Technikerstraße 25/8, Innsbruck, A-6020, Austria*

⁹*European Southern Observatory, Karl-Schwarzschild-Str. 2, D-85748 Garching, Germany*

¹⁰*Univ. Lyon, ENS de Lyon, Univ. Lyon 1, CNRS, Centre de Recherche Astrophysique de Lyon, UMR5574, F-69007 Lyon, France*

¹¹*Department of Astronomy, Yonsei University, Seoul 03722, Republic of Korea*

(Received —; Revised —; Accepted —)

ABSTRACT

Ultra-diffuse galaxies (UDGs) are very low-surface brightness galaxies with large effective radii. Spectroscopic measurements of a few UDGs have revealed a low dark matter content, based on the internal motion of stars or globular clusters (GCs). This is in contrast to the large number of GCs found for these systems, from which it would be expected to correspond to a large dark matter halo mass. Here we present HST+ACS observations for the UDG MATLAS-2019 in the NGC 5846 group. Using the *F606W* and *F814W* filters, we trace the GC population two magnitudes below the peak of the GC luminosity function (GCLF). Employing Bayesian considerations, we identify 26 ± 6 GCs associated with the dwarf, yielding a large specific frequency of $S_N = 58 \pm 14$. We use the turnover of the GCLF to derive a distance of 21 ± 2 Mpc, which is consistent with the NGC 5846 group of galaxies. Due to the superior image quality of the HST, we are able to resolve the GCs and measure their sizes, which are consistent with the sizes of GCs around Local Group galaxies. Using the linear relation between the total mass of galaxies and of GCs, we derive a halo mass of $0.9 \pm 0.2 \times 10^{11} M_\odot$ ($M_\odot/L_\odot > 1000$). The high abundance of GCs, together with the small uncertainties, make MATLAS-2019 one of the most extreme UDGs, which likely sets an upper limit of the number of GCs for UDGs.

Keywords: editorials, notices — miscellaneous — catalogs — surveys

1. INTRODUCTION

Dwarf galaxies are by far the most numerous galaxies in the Universe (Ferguson & Binggeli 1994) and exist in all kinds of environments, from dense clusters to isolated voids (e.g. Binggeli et al. 1990; Rekola et al. 2005; Kim & Jerjen 2015; Müller et al. 2017; Makarov et al. 2017).

They are thought to be the most dark matter dominated objects, with the most extreme cases consisting of more than 99% of this elusive material (Walker et al. 2007; McGaugh & Wolf 2010; Collins et al. 2020). A subsample of the dwarf galaxy population is called ultra-diffuse galaxies (UDGs), a term coined by van Dokkum et al. (2015). UDGs are characterized by their large effective radii and very low-surface brightnesses. While their existence has been known since the 1980's (e.g., Sandage & Binggeli 1984; McGaugh & Bothun 1994; Dalcanton et al. 1997; Conselice et al. 2003; de Rijcke

et al. 2009; Crnojević et al. 2014; Penny et al. 2014), recently they have become the focus of enhanced attention by the astronomical community, due to the discovery of hundreds of these objects ranging from cluster to group environments (e.g., Koda et al. 2015; Mihos et al. 2015; Martínez-Delgado et al. 2016; Mihos et al. 2017; van der Burg et al. 2017; Venhola et al. 2017; Müller et al. 2018, 2021; Zaritsky et al. 2019; Lim et al. 2020; Habas et al. 2020; Iodice et al. 2020), and as a result unlocked the potential to study these objects in unprecedented detail.

Due to their diffuse nature, UDGs are an excellent probe of the underlying gravitational potential (e.g., Danieli et al. 2019; Bílek et al. 2019; Mancera Piña et al. 2019; Gannon et al. 2020). Such studies have been conducted on some specific UDGs, like the two UDGs [KKs2000] 04/NGC 1052-DF2 (Karachentsev et al. 2000; van Dokkum et al. 2018a) and NGC 1052-DF4 (van Dokkum et al. 2019a) in the NGC 1052 group of galaxies, NGC 5846-UDG1/MATLAS-2019 (Forbes et al. 2019; Habas et al. 2020) in the NGC 5831 group of galaxies, VCC 1287 (Binggeli et al. 1985; Beasley et al. 2016) in the Virgo cluster, and DF17 (Peng & Lim 2016) and DF44 (van Dokkum et al. 2016) in the Coma cluster. The extraction of the stellar velocity dispersion of the body of the galaxy or the velocity dispersion of the globular cluster (GC) population associated to the UDGs has enabled the study of the dark matter content of the galaxies (e.g., van Dokkum et al. 2018a, 2019a; Chilingarian et al. 2019; Emsellem et al. 2019; Müller et al. 2020; Gannon et al. 2020). While the measurements at face values can be interpreted as an absence of dark matter in these galaxies, both the observational (Martin et al. 2018) and systematic uncertainties (Laporte et al. 2019) are too large to yet be conclusive.

Two main mechanisms have been proposed for the formation of UDGs: either they are failed Milky Way like galaxies which couldn't build up their baryonic content (e.g., van Dokkum et al. 2016; Peng & Lim 2016; Toloba et al. 2018), or they are dwarf galaxies extended to larger radii, which were puffed up through tidal effects (e.g. tidal interactions or tidal heatings, Ogiya 2018; Toloba et al. 2018; Carleton et al. 2021). These two scenarios result in quite different dark matter halo masses for the galaxies. X-Ray observations of multiple UDGs (Kovács et al. 2019), as well as their location in the scaling relations (Habas et al. 2020), have revealed that the majority of UDGs are consistent with being normal dwarf galaxies, adding evidence that UDGs are simply the extension of the dwarf galaxy population towards larger radii. Still, this does not exclude the possibility that some UDGs could belong to the former group of failed Milky Way galaxies. One archetypal UDG –

namely DF44 in the Coma cluster – has been studied in detail with spectroscopy (van Dokkum et al. 2016, 2019b), deep imaging (van Dokkum et al. 2017), and X-ray observations (Bogdan 2020). While initial claims (van Dokkum et al. 2016) pointed it towards the group of failed galaxies – based on a high count of GCs, as well as an atypical mass for a dwarf galaxy – these claims have been weakened by more recent studies (Amorisco et al. 2018; van Dokkum et al. 2019b; Saifollahi et al. 2020; Bogdan 2020).

One way to indirectly infer the mass of a galaxy without measuring the internal stellar dynamics is through the number of GCs (Blakeslee et al. 1997; Spitler & Forbes 2009; Georgiev et al. 2010; Hudson et al. 2014; Beasley et al. 2016; Burkert & Forbes 2020). In a Λ CDM framework, the dark matter halos of galaxies are directly correlated with the abundance of GCs, i.e. a high number of GCs indicates a vast halo of dark matter. Several studies based on deep imaging have estimated the number of GCs associated to UDGs (Lim et al. 2018; Amorisco et al. 2018; Prole et al. 2019). They again indicate that UDGs are consistent with being from the dwarf galaxy population, but due to the statistical nature of these studies, the scatter and uncertainties are large. Furthermore, these studies were mainly conducted in dense cluster environments, and may not be representative of the full UDG population.

The low-mass environments of groups of galaxies are still uncharted territory. This has started to change in recent years (e.g., Chiboucas et al. 2009; Müller et al. 2015, 2017; Javanmardi et al. 2016; Park et al. 2017; Danieli et al. 2018; Carlsten et al. 2020; Müller & Jerjen 2020). Among these campaigns is the Mass Assembly of early Type galaxies with their fine Structures (MATLAS, Duc et al. 2015; Duc 2020; Bílek et al. 2020) survey, a MegaCam based survey of over 200 nearby early type galaxies within 45 Mpc. The multi-color imaging in the *ugri*-filters and good image quality made it possible to simultaneously detect dwarf galaxies and GCs. Over 2000 dwarfs have been discovered (Habas et al. 2020), with $\sim 5\%$ of them being UDGs (Marleau et al., accepted). The UDG with the highest number of GCs in this systematic survey is MATLAS-2019 (Marleau et al., accepted). This UDG has an effective surface brightness of ≈ 25.1 mag arcsec $^{-2}$ in the *g* band, an effective radius of $17.2''$ ($= 2.2$ kpc, for the previously assumed distance of $d = 26$ Mpc, corresponding to the center of the NGC 5846 group), and a systemic velocity of 2156 ± 9 km s $^{-1}$ (Müller et al. 2020), which is consistent with the NGC 5846 group of galaxies (Egenthaler & Zeilinger 2010, see also Fig. 1 in Müller et al. 2020). Spectroscopic follow-up observations with MUSE

have confirmed that at least 11 GCs are associated with MATLAS-2019 (Müller et al. 2020), which are all consistent with being metal-poor and old. Intriguingly, at the putative distance to the host group, the brightest GC would be almost as bright as ω Cen, which is unexpectedly bright for such a low-surface brightness object. This can also be interpreted as further evidence that ω Cen is an accreted GC from a bright, now-disrupted dwarf galaxy (Majewski et al. 2000). However, the data was too shallow to trace the GC population to the faint end. A similar case is NGC 1052-DF2, with the claim that it has a population of too-luminous GCs (van Dokkum et al. 2018b). Either these GCs are indeed too bright, or they are just the tip of the iceberg, i.e. the bright tail of a largely populated GC luminosity function (GCLF). In this work, we present *Hubble Space Telescope* (HST) imaging of MATLAS-2019 to study its GC population by tracing the full GCLF.

2. OBSERVATIONS AND DATA REDUCTION

Our HST images were obtained through a single orbit in the Mid-Cycle 27 program GO-16082, (PI: Müller) to observe the UDG MATLAS-2019. This galaxy was first identified in Mahdavi et al. (2005) and named N5846-156, and has been identified in the MATLAS survey (Habas et al. 2020), as well as independently reported in the VST Early-type GALaxy Survey (VEGAS, Forbes et al. 2019). We observed MATLAS-2019 with the HST Advanced Camera for Surveys (ACS) in the F606W and F814W filters. The galaxy itself was placed at the center of one of the CCDs to maximize a suitable background/control sample. Two dithered images (separated by $0.5''$) of 515s each were taken in each filter. We used the final, reduced CTE-corrected (Charge Transfer Efficiency corrected) *.drc.fits* images produced by the standard pipeline and used the VEGAmag zeropoints provided by the ACS online documentation¹.

We performed aperture photometry on each filter with the python package photutils (Bradley et al. 2020). To remove the smooth light profile of the galaxy, we have modelled and subtracted it with GALFIT (Peng et al. 2002). The center of the galaxy is estimated to be at 15:05:20.34, +01:48:44.9. Then, we ran sep (Barbary 2016), the Source Extractor (Bertin & Arnouts 1996) implementation in python, with a 3σ threshold and a minimum of 5 adjacent pixels, to create a catalog of objects. On this catalog we made a first cut, namely we rejected all sources with a detected radius smaller than 3 px or an ellipticity larger than 0.2. This removed

noise peaks as well as elongated objects such as background galaxies. We performed photometry on the detections in the catalog with a circular aperture with a radius of 3 px. The median background value was estimated in an annulus with inner and outer radii of 8 px and 23 px, respectively, employing a 3σ clipping, and was subtracted from the photometry of the object. Aperture corrections were applied according to the ACS documentation². The $F606W$ and $F814W$ magnitudes were corrected for extinction ($A_{F606W} = 0.131$ mag and $A_{F814W} = 0.081$ mag) according to the extinction calculator tool on NED³ (using Schlafly & Finkbeiner 2011). We then matched the catalogs in the two filters with a 0.5 arcsec tolerance. Finally, we applied a magnitude cut in the $F606W$ band of $22.0 < F606W < 26.2$ mag, as well as a $(F606W - F814W)_0$ color cut of $0.5 < (F606W - F814W)_0 < 0.9$ mag, motivated by the range of expected magnitudes and colors of GCs. From this we generated a catalog of 241 GC-like sources over the entire ACS FOV. Of these, we extract a sample of $N_{tot} = 49$ GC candidates located within $1.75 r_{eff}$ of the galaxy center (this optimal aperture size is derived in Section 3.3). The GC candidates are presented in Fig. 1 and Fig. 2. As a reference background field, we use an area of $100 < x < 4090$ and $100 < y < 2020$ pixels on the second chip, containing 74 sources in our catalog. This area is well outside of $3 r_{eff}$ (see Fig. 1).

To assess our completeness and photometric errors we have injected artificial point sources in the HST data and re-run our detection and photometry pipeline. For that we have created a PSF model using 14 bright, isolated stars on the frame. Artificial stars were added on a evenly-spaced grid with a separation of 70 pixels. This gives ≈ 2500 injected objects. We have repeated this for a magnitude range between 21 and 28.3 in both filters. To obtain the completeness, we have compared the number of injected vs. number of detected objects. In order to not count real objects as successfully detected artificial objects, we have provided Source Extractor with the original segmentation map of the image as a mask. For the photometric error we have compared the injected and extracted magnitudes. The completeness drops below 95% at $F606W = 26.74$ mag and $F814W = 25.82$ mag. The results of our artificial star experiments are shown in Fig. 3. To test whether the light from MATLAS-2019 impacts the performance we consider the detections within one effective radius of the

¹ <https://www.stsci.edu/hst/instrumentation/acs/data-analysis/zeropoints>.

² <https://www.stsci.edu/hst/instrumentation/acs/data-analysis/aperture-corrections>.

³ http://ned.ipac.caltech.edu/extinction_calculator.

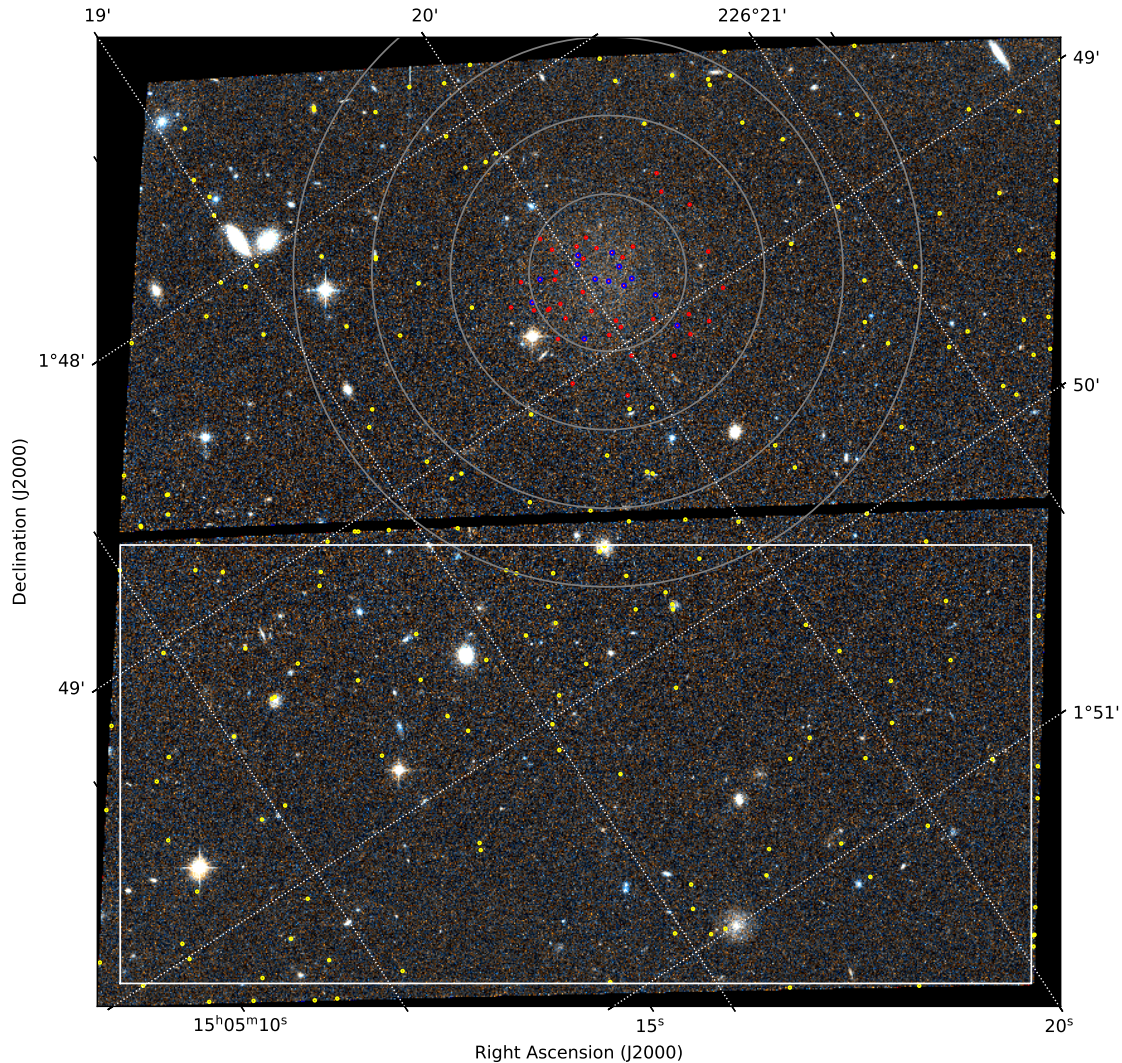


Figure 1. The full ACS field of view of our HST observations. In red we indicate the detected GC candidates, in blue the confirmed GCs from MUSE observations, and in yellow we show the selected field GC candidates. The gray circles are multiples of the effective radius, starting with $1 r_{eff}$. The white box indicates the reference field.

galaxy separately. Within this radius, ≈ 70 objects are injected per iteration. From these we can again construct a completeness curve. Apart from the the curve being more noisy – due to having less objects to work with – we find no difference in the shape and the reached completeness limit.

To convert the HST $F606W$ and $F814W$ magnitudes into the standard BVI system, we employed the transformations provided by Harris (2018) and assumed a $(V - I)_0 = 0.9$ mag color for the GCs.

$$V = F606W + 0.15(V - I)_0 \quad (1)$$

$$I = F814W - 0.13 + 0.108(V - I)_0 \quad (2)$$

Due to the superior image quality of the HST the GCs in our data are partially resolved. To measure their half light sizes (r_h), core sizes (r_c) and tidal radii (r_t), we have employed GALFIT using a Sérsic profile and a King profile, respectively, which were convolved with the PSF model. For the fitting, we let the Sérsic index be a free parameter smaller than five, which helped reduce crashes. All photometric properties are compiled in Table 3.

3. PROPERTIES OF THE GLOBULAR CLUSTER POPULATION

3.1. Globular Cluster Luminosity Function

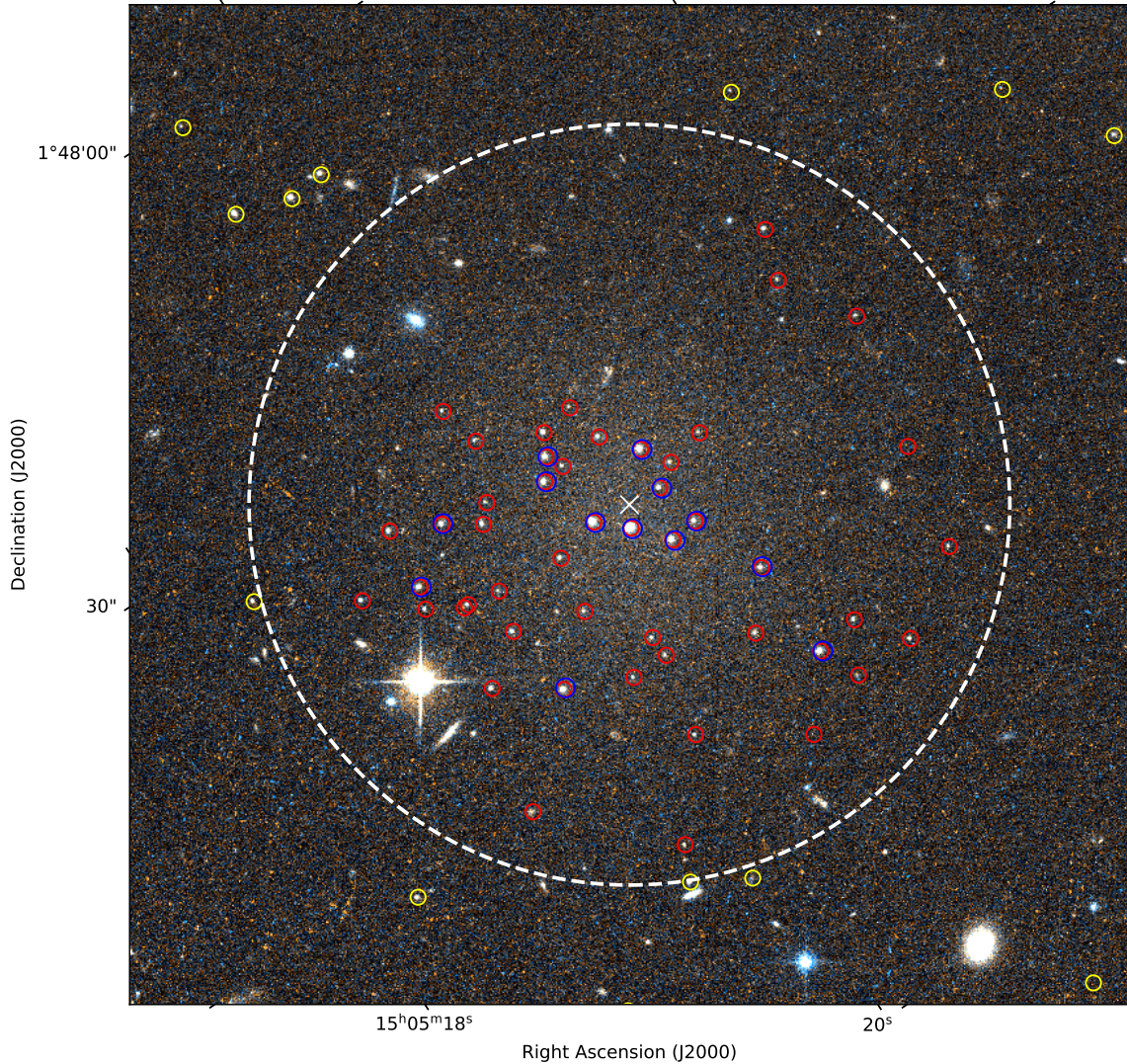


Figure 2. The zoom in view of our HST observations. The dashed white line corresponds to the radius where the GC candidate count drops to a background level (i.e. at $1.75 r_{eff}$), corresponding to our selection radius. The white cross indicates the galaxy center. In red we indicate the detected GC candidates, in blue the confirmed GCs from MUSE observations, and in yellow we show the selected field GC candidates. One side is $\approx 80''$.

In the following we will model the GCLF using Bayesian considerations. For the GCLF we assume a log-normal distribution \mathcal{G}_V in luminosity:

$$\mathcal{G}_{V,j}(m_V, \delta_{V,err}) = \frac{1}{\sqrt{2\pi}} \frac{1}{\sigma_{obs}} \exp \frac{-(m_{V,j} - \mu_V)^2}{2\sigma_{obs}^2}, \quad (3)$$

with

$$\sigma_{obs} = \sigma_{V,j}^2 + \delta_{V,err}^2. \quad (4)$$

The magnitude of the GC candidate j is given by $m_{V,j}$. The total width σ_{obs} is the combination of the intrinsic width of the GCLF σ_V and the mean error $\delta_{V,err}$ of all the GCs. To model the background contamination \mathcal{B}_V we use all GC-like objects outside $1.75 r_{eff}$ to create a histogram with a bin size of 0.5 mag. We

then interpolate the midpoints of the bins to create \mathcal{B}_V . Similarly, we model the color of the GC distribution with a normal distribution $\mathcal{G}_{(V-I)_0}$ and derive the background contamination $\mathcal{B}_{(V-I)_0}$ from all the GC-like objects outside $1.75 r_{eff}$. We assume a normal distribution for the colors of the GCs of MATLAS-2019 because when we inspected the color magnitude diagram (CMD, see Sec 3.2), we found that the color distribution is strikingly unimodal. In general, this doesn't need to be the case.

We use a Plummer profile \mathcal{P} to model the spatial distribution of the GCs:

$$\mathcal{P}(r)_j = \frac{1}{\pi} \frac{1}{r_{GC}^2 (1 + r_j^2/r_{GC}^2)^2}, \quad (5)$$

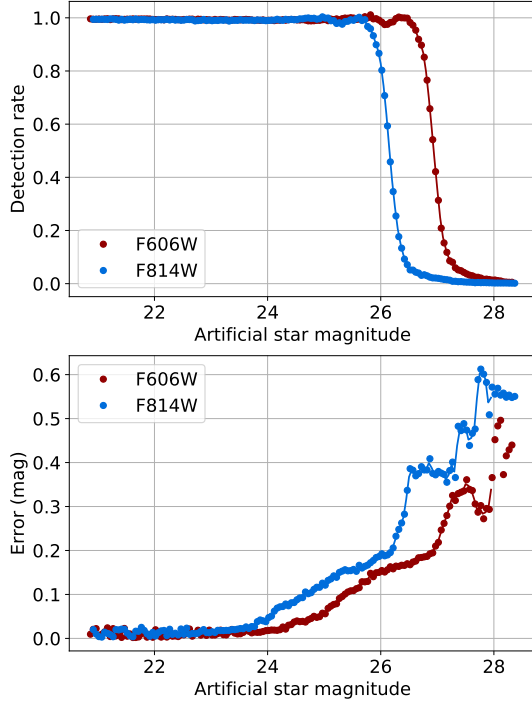


Figure 3. Results of the artificial star experiments. The top panel shows the detection rate, the bottom panel the mean uncertainty of the recovered artificial stars.

where r_j is the galactocentric distance of the GC candidate j and r_{GC} is the half number radius of the GC system, which is a free parameter. To be consistent in the dimensions, we multiply this density with the number of GCs N_{GC} associated with the galaxy:

$$\Sigma(r)_j = N_{GC} \cdot \mathcal{P}(r)_j \quad (6)$$

The contamination c out to the outermost GC candidate (having the radius R_{out}) is given by:

$$c = \frac{N - N_{GC}}{\pi R_{out}^2}. \quad (7)$$

Finally, the likelihood for a source j in our catalog is given by:

$$L_j = \frac{\Sigma_j \cdot \mathcal{G}_{V,j} \mathcal{G}_{(V-I)_0,j} + c \cdot \mathcal{B}_{V,j} \mathcal{B}_{(V-I)_0,j}}{\Sigma_j + c}. \quad (8)$$

The parameters we are marginalizing over are μ_V and σ_V , i.e. the peak and the width of the GCLF; the number of true GCs N_{GC} associated with MATLAS-2019; the half number radius r_{GC} of the GC system; and $\mu_{(V-I)_0}$ and $\sigma_{(V-I)_0}$, i.e. the peak and the width of the color distribution. As priors we use flat priors, namely for σ_V we allow values between 0 and 2 mag, which are well motivated by observations (Rejkuba 2012); for μ we

Table 1. Priors for our Markov Chain Monte Carlo.

Parameter	Prior
σ_V	$0 < \sigma_V < 2$
μ_V	$22 < \mu_V < 26.8$
N_{GC}	$0 < N_{GC} < 49$
R_{out}	$0 < R_{out} < 30$
$(V - I)_0$	$0.6 < (V - I)_0 < 1.1$
$\sigma_{(V-I)_0}$	$0.0 < \sigma_{(V-I)_0}$

impose the condition that it must be within our magnitude range (i.e being between 22 and 26.8 mag); for N_{GC} we impose that the number must be between 0 and the number of detected sources within our aperture ($N = 49$); for r_{GC} we set them to be between 0 and R_{out} (i.e. $30''$); and for the colors we demand that they must be between $0.6 < (V - I)_0 < 1.1$ mag and that $\sigma_{(V-I)_0}$ must be larger than 0. A summary of the prior constraints is given in Table 1.

To estimate the posterior distributions for these six parameters (μ_V , σ_V , N_{GC} , r_{GC} , $\mu_{(V-I)_0}$, and $\sigma_{(V-I)_0}$) we employ a Markov Chain Monte Carlo (MCMC) algorithm (Goodman & Weare 2010) implemented through the python package emcee (Foreman-Mackey et al. 2013). As a first guess for the parameters, we use a maximum likelihood method implemented in scipy (i.e. minimize from the scipy.optimize module), which yields $\mu_V = 23.99$ mag, $\sigma_V = 0.81$ mag, $N_{GC} = 24.2$, and $r_{GC} = 13.7''$, $\mu_{(V-I)_0} = 0.87$ mag, and $\sigma_{(V-I)_0} = 0.03$ mag. For the MCMC we use 100 walkers with 10 000 steps along the chains, with a burn-in of 1000 steps. For the peak of the GCLF we derive $\mu_V = 23.99 \pm 0.24$ mag, for the width of the GCLF $\sigma_V = 0.88 \pm 0.16$ mag, for the number of GCs $N_{GC} = 26.0 \pm 6.0$, for the half number radius $r_{GC} = 13.4_{-5.8}^{+7.5}''$, and for the color a mean of $(V - I)_0 = 0.87 \pm 0.01$ mag with a spread of $\sigma_{(V-I)_0} = 0.03 \pm 0.01$ mag. The posteriors are well-behaved and presented in Fig 4.

The histogram of the GC candidates within $1.75 r_{eff}$ and the best-fitting model are presented in Fig 5. The peak of the GCLF puts the galaxy at $20.6_{-2.1}^{+2.3}$ Mpc (assuming the peak of the GCLF is at -7.6 ± 0.1 mag, Rejkuba 2012). This is consistent with the distance of the NGC 5846 group (having a mean of 26 Mpc, Cappellari et al. 2011, but having giant galaxies within a spread of $\approx \pm 5$ Mpc). Our MCMC modelling reveals a large number of GCs for such a low-luminosity dwarf. The brightest GCs are consistent with the normal bright end of the GCLF at the distance of the NGC 5846 group, indicating there are no over-luminous GCs present in this galaxy, as has been suggested (Müller et al. 2020). Rather, the

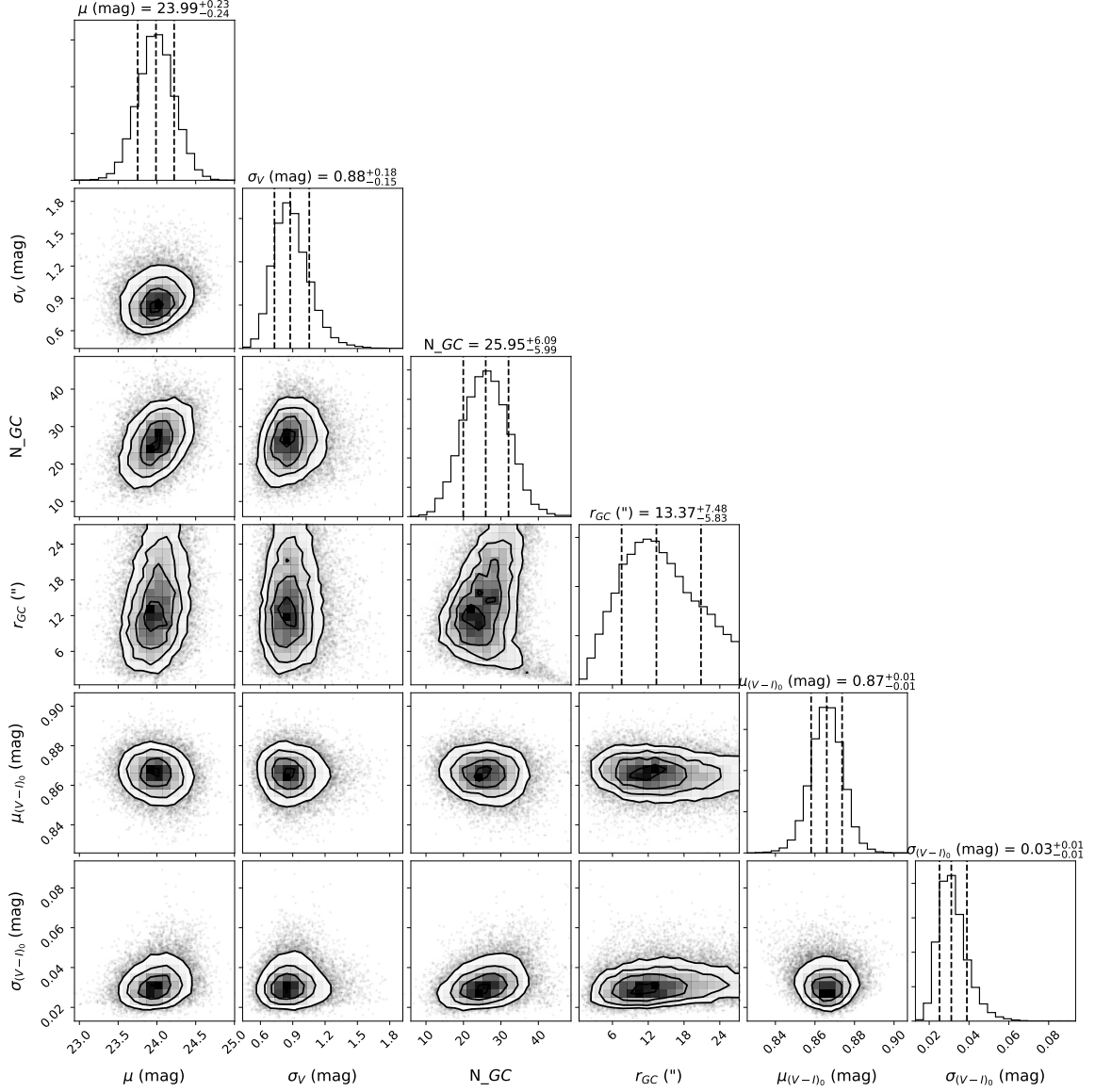


Figure 4. The posterior distributions from our MCMC modelling with its six free parameters (μ_V , σ_V , N_{GC} , r_{GC} , $\mu_{(V-I)_0}$, and $\sigma_{(V-I)_0}$).

GCLF is best explained by a large population of GCs for a galaxy of this luminosity. For reference, in Fig. 5 we further show the histogram of the detected GC candidates within and outside of the galactic aperture.

As a check, we estimate the numbers of GCs expected in our aperture of the size $1.75 r_{eff}$, when considering the contamination estimated on our reference background field. With an area of 5.3 arcmin and 74 GC-like sources in this reference background area, we expect ≈ 13 GC candidates in our aperture to be interlopers. In other words, there should be an over-density 36 ± 6 detection within our aperture assuming Poissonian noise for the estimation of the uncertainty. This number is larger than the number of GCs ($N_{GC} = 26 \pm 6$) esti-

mated by our MCMC scheme. This can be explained by Poisson noise: the mode or median value of a Poisson distribution is lower than its expectation value, meaning that when we estimate the contamination from our background field we will likely underestimate the number of contaminants (i.e. overestimate the number of GCs associated with the dwarf). However, within the uncertainties, these numbers are still consistent.

To test that this difference between our MCMC approach and the overdensity estimate of the number of GCs is not due to our model, we produced a synthetic data set where we had the control over the number of GCs and the other parameters of interest. For this purpose, we used the same number of detections as for

our analysis. To create the background, we used our background luminosity and color model together with a random position to draw the data points. For our synthetic GCs, we drew their luminosities from a gaussian with the peak and standard deviation as our estimated values ($\mu = 24$ mag and $\sigma = 0.9$ mag), with a color of $(V - I) = 0.9$ mag, and a positions drawn from the Plummer profile with the estimated value of $r_{GC} = 12.6$ arcsec. All the remaining inputs were kept the same. With this setup, we were able to recover all input parameters within their uncertainties, with slightly overestimating the number of GCs (on average getting 28.9 ± 2.2 GCs instead of 26).

3.2. Luminosities, colors, and sizes

In Fig. 6 we present the CMDs of our observations. We considered three cases: all detected point sources within i) one effective radius (r_{eff}), ii) between 1 and $2r_{eff}$, and iii) outside of $2r_{eff}$. Remarkably, within $1r_{eff}$ the GCs follow an extremely tight sequence. All confirmed GCs from our MUSE observations (Müller et al. 2020) within $1r_{eff}$ are located within this sequence. For the other two CMDs, the color scatter of the GCs increases, which is due to an increase of the background contamination. This indicates that the GC population contribution drops after one effective radius and the contamination by background/foreground sources increases. This is a similar trend as seen the GC population of DF44, where the GC population drops significantly after one effective radius (Saifollahi et al. 2020). We will quantify this further in the next subsection.

For most GC candidates, the core radius is systematically smaller than the half-light radius, as has been found for Cen A GCs (Harris et al. 2002). As a sanity check, the fraction between the tidal radius and the core radius under a logarithm with the base of 10 should roughly be between 1 and 2 for confirmed GCs (Harris et al. 2002). This is the case for most of the GC candidates here, especially within the given large errors of these difficult observations. The sizes are not used in the selection for the GC candidacy though, making them an independent property. This suggests that most of the GC candidates selected by their magnitudes and colors are also GC-like in their morphology and are therefore reasonable GC candidates.

In Fig. 7 (left panel) we plot the sizes (r_h) of the GCs as functions of luminosity and color. Most of the GC candidates are smaller than 10 pc, which is well expected from studies of the sizes of Milky Way GCs (Harris 2010). All of our spectroscopically confirmed GCs are in this range. Some of the faint GC candidates, however, have larger sizes than the brighter GCs. This could have

a few explanations. The fainter GC candidates have a lower S/N, which could systematically increase their sizes due to modelling uncertainties (which are not well captured by galfit). Alternatively, and more likely, they are the background objects contaminating our selection. We expect $N_{tot} - N_{GC} = 23$ objects in our catalog to be background interlopers. It is also possible a few of these objects could be faint, diffuse GCs, much like those seen in M31 (Huxor et al. 2014) with r_h values up to 30-35 pc. Up to five GC candidates (including their uncertainties) could have half light radii larger than the one of Crater-I (i.e. $r_{eff} = 20$ pc, Torrealba et al. 2016) – which is one of the most extreme GCs in terms of size associated with the Milky Way (Voggel et al. 2016) – and could therefore be such extreme GCs. However, until spectroscopically confirmed, it is more likely that those are the expected interlopers.

In Fig. 7 (right panel) we also plot the GC candidates of MATLAS-2019 compared to other known GCs from the Local Group (Peacock et al. 2010; Harris 2010), as well as ultra-compact dwarfs (UCDs, Hilker et al. 1999) in the Virgo cluster (Liu et al. 2015, 2020). The particular cases of Crater-I and Pal 14, the largest Milky Way GC, are highlighted in the figure. For the UCD FCC 47-UCD1 (Fahrion et al. 2019) in the Fornax cluster, Fahrion et al. (2019) (among others) have suggested that it could originate from the brightest star cluster in the progenitor galaxy and was accreted through a minor merger, and it could be interesting to see if we would have such a compact stellar object in our sample. While most of the GC candidates associated with MATLAS-2019 follow the distribution of the Local Group GCs, one GC in particular – the brightest GC in our sample dubbed GC6 in Müller et al. (2020) – is approaching the UCD regime, with a size of $r_{eff} = 6.7 \pm 0.2$ pc and an absolute magnitude of -9.2 mag in the V band. In Table 3, GC6 is number 29. We note that the GCLF peak distance prefers a value of 21 Mpc, while the velocity of the galaxy rather puts it at 25 to 30 Mpc. If the dwarf is at a larger distance, the sizes and luminosities of the GCs would increase, and GC6 would be closer to the UCD regime ($r_{eff} \approx 10$ pc and $M_V \approx -10$ mag). However, GC6 would fall out of the selection of UCDs in the Virgo cluster – independent of whether the dwarf is at 21 or 30 Mpc –, with the GC being too small to be considered a UCD. So with their selection criteria, GC6 is not a UCD. Forbes et al. 2019 suggested that this GC is a nuclear star cluster, based on its brightness and central placement within the galaxy. Its velocity is similar to that of the stellar body (Müller et al. 2020; Forbes et al. 2021), further supporting this assessment.

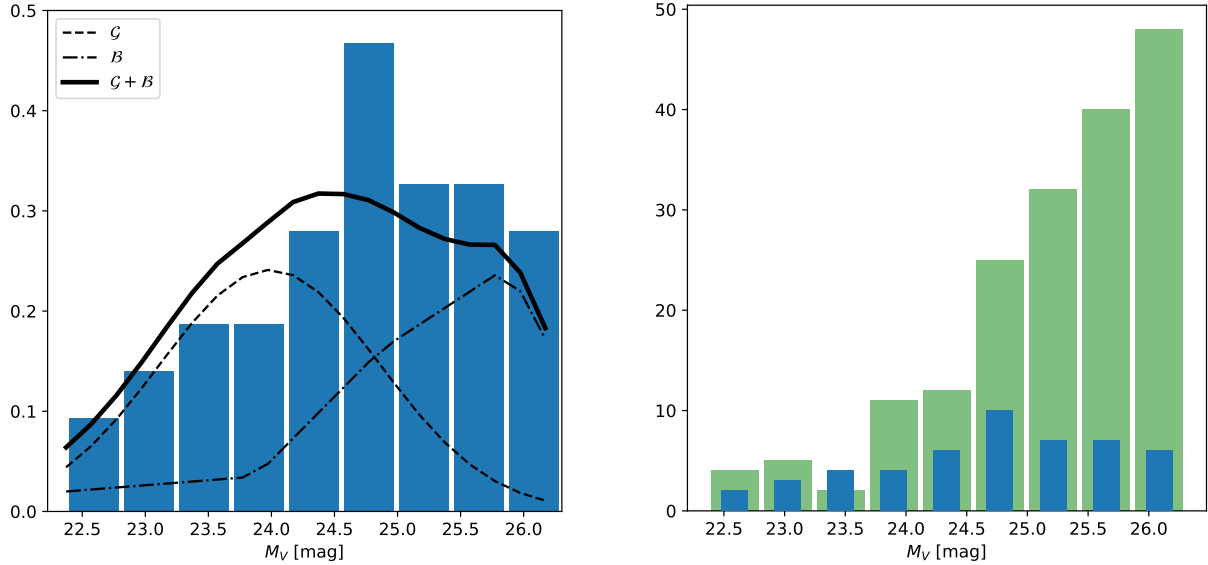


Figure 5. Left: The normalized histogram of the V_0 band magnitudes of the GC candidates within $1.75 r_{eff}$. The dashed line corresponds to the GCLF, the dash-dotted line to the background model, and the thick line to the combination of the two. Right: The histogram of the V_0 band magnitudes of GC candidates within the $1.75 r_{eff}$ aperture (blue) and outside of this aperture (green).

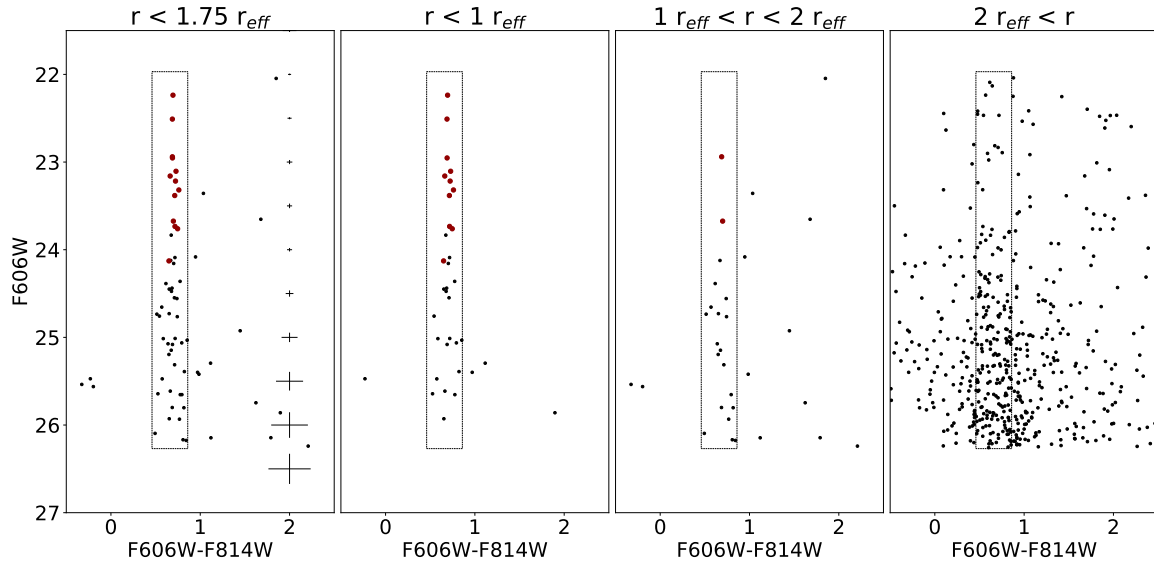


Figure 6. The CMD of detected sources within $1.75 r_{eff}$ (left), corresponding to the full extent of the GC system; within $1 r_{eff}$ (middle left); within 1 and $2 r_{eff}$ (middle right); and outside of 2 (right). The dotted line corresponds to our selection of GCs. In the left panel, we indicate in red the spectroscopically confirmed GCs from Müller et al. (2020).

3.3. Radial profile

In the following, we quantify the radial extent of the GC distribution. For this, we counted the number of GCs per area in increasing annuli of multiples of $0.25 r_{eff}$. The results are presented in Fig. 8. At $1 r_{eff}$, the GC density is at roughly 10% compared to the innermost circle, and after $1.75 r_{eff}$, the GC count drops to the background level (being calculated from the density

of GC candidates on the reference field on the second chip). While most of the GCs reside within one effective radius, the GC population extends to roughly two effective radii, or ≈ 3 kpc.

Notably, there is a mass segregation apparent in the GC population of MATLAS-2019. This is qualitatively evident in Fig. 2, where we present the zoom-in of the HST observation within two effective radii. All the

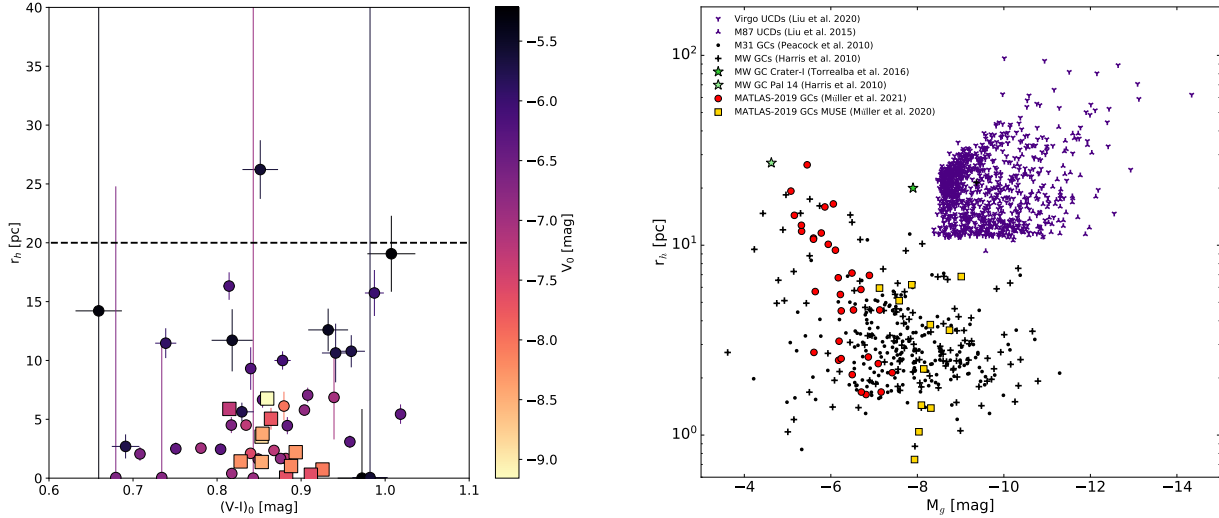


Figure 7. Left: The size of the GCs as a function of their $(V-I)_0$ color. The points are further shaded based on their luminosity. The spectroscopically confirmed GCs (Müller et al. 2020) are represented with the squares. The dashed line indicates the size of Crater-I (Torrealba et al. 2016), an extreme example of an extended GC in the Milky Way. Right: The size of the GCs as a function of their luminosity and compared to Local Group GCs (Peacock et al. 2010; Harris 2010) and Virgo cluster UCDs (Liu et al. 2015, 2020). The red filled circles indicate the GCs associated with MATLAS-2019 and the gold filled squares are those spectroscopically confirmed with MUSE.

bright GCs are clustered towards the center of the dwarf. Quantitatively, this is shown in Fig. 8, where we split the density profiles into faint and bright GCs (with a magnitude cut at 23.1 mag, which corresponds to the 1σ of the GCLF at the bright end). The density profile of the bright GCs is centrally peaked and quickly drops to zero within $0.75 r_{eff}$, while the density profile of the faint GCs is more extended (up to $1.75 r_{eff}$) and less peaked. However, the contamination of background galaxies will increase at the faint end, so this could bias the signal. Another caveat might be a drop in completeness towards the center of the galaxy. As discussed previously, the photometric incompleteness near the center of the galaxy does not appear to have a significant impact on source detection. Ultimately, spectroscopic follow-up observations are needed to confirm this mass segregation.

4. SPECIFIC FREQUENCY

Is the abundance of GCs associated to MATLAS-2019 consistent with other UDGs and dwarf galaxies? One way to assess the number of GCs as a function of the brightness of the host galaxy is with the specific frequency S_N (Harris & van den Bergh 1981). It is calculated as:

$$S_N = N_{GC} \cdot 10^{0.4(M_V+15)} \quad (9)$$

The peak of the GCLF yields a distance modulus of $m - M = 31.57$ mag. The apparent and absolute magnitudes of MATLAS-2019 are $m_V = 17.69$ mag and $M_V = -14.1 \pm 0.2$ mag, respectively (Poulain et al.

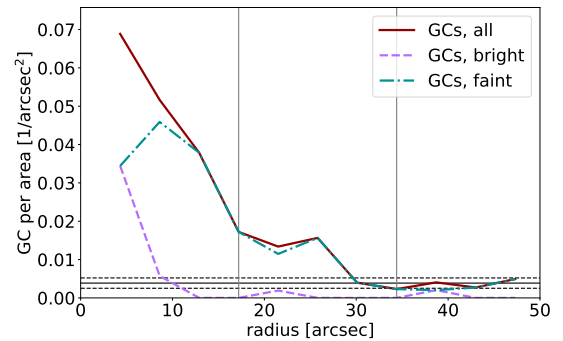


Figure 8. The GC density (red line) in increasing annuli of radii of $0.25 r_{eff}$. The densities of bright GCs and fainter GCs are marked with the violet dashed line and cyan dash-dotted line, respectively. The vertical lines indicate one and two effective radii, respectively. The horizontal straight and dashed black lines represents to the background GC density on chip two of the ACS field.

2021). This gives a specific frequency of $S_N = 58 \pm 14$, where the error is a combination from the uncertainty in the absolute magnitude (± 0.23 mag) and the number of GCs (± 6).

How does the specific frequency of MATLAS-2019 compare to other low-luminosity galaxies? In Fig. 9 we show the specific frequency as a function of the luminosity and surface brightness of the galaxies. Several statistical studies of dwarf galaxies and UDGs (Lim et al. 2018; Prole et al. 2019) have revealed a large scatter in the specific frequency at the faint end. Lim et al. (2018) noted that for the same luminosity, UDGs have

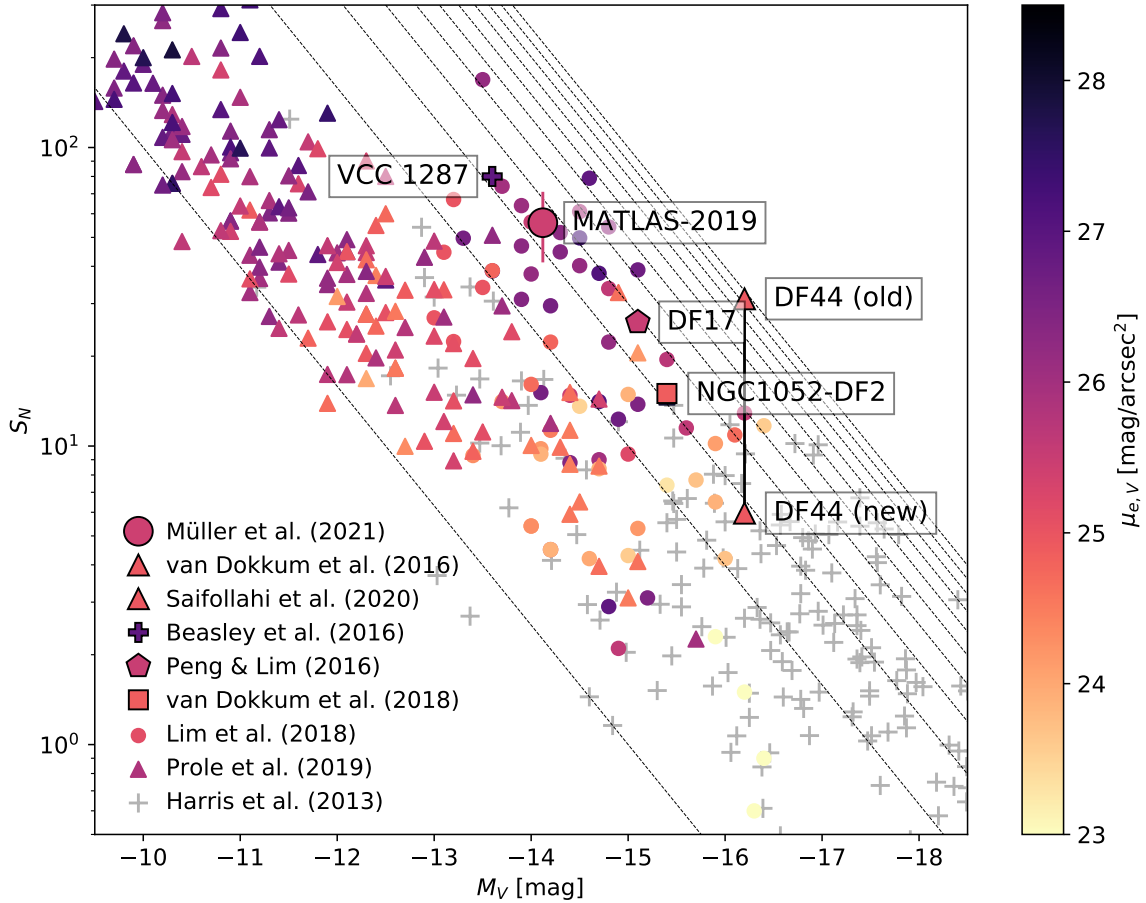


Figure 9. The specific frequency of nearby galaxies (Harris et al. 2013), Coma cluster dwarfs (Lim et al. 2018), Fornax cluster dwarfs (Prole et al. 2019), and the UDGs MATLAS-2019 (this work), DF44 (Saifollahi et al. 2020), DF17 (Peng & Lim 2016), VCC1287 (Beasley et al. 2016), and NGC1052-DF2 (van Dokkum et al. 2018b). The color bar indicates the effective surface brightness of the galaxies. The dashed lines correspond to specific frequencies with a constant number of GCs of 1, 10, 20, ..., 90, 100.

a lower surface brightness and higher specific frequency than typical dwarf galaxies. MATLAS-2019 follows this trend. It has a high specific frequency for its luminosity and has one of the largest counts of GCs in such systems. While MATLAS-2019 doesn't stand out as having the highest specific frequency at first sight (some of the Lim et al. 2018 UDGs have a higher S_N value), a direct comparison between the literature UDG sample and MATLAS-2019 is tricky, mainly due to the high uncertainty of the number of GCs in the literature, as well as different approaches in counting the number of GCs. We discuss the caveats of comparing the number of GCs in the following.

For UDGs with a high specific frequency in the Lim et al. (2018) UDG sample (i.e. UDGs with $S_N > 30$), the median uncertainty is 33, where in the Prole et al. (2019) sample the median uncertainty is 11. Based on the large uncertainties of those two surveys, it is expected to find some UDGs with a high number of GCs

due to stochasticity. The larger error of the specific frequency estimation in these works can be explained by the fact that the dwarf galaxies studied there are either farther in the background or have been observed with ground-based facilities, where the image quality becomes an issue. In comparison to the Lim et al. (2018) sample, with our observations we achieve an uncertainty of 14, i.e. at a $\approx 25\%$ level.

There are also different selection functions used in the literature. Lim et al. (2018) had to correct for their incompleteness of the GC population – the Coma dwarfs are four times farther away than MATLAS-2019, meaning that the full GCLF could not be traced. They selected the GCs within $1.5r_{eff}$, multiplied by a factor 2 to correct for the full extent of the GC population (i.e. assuming that the half of the GC population will be within $1.5r_{eff}$), and an additional factor 2 for the incompleteness of the GCLF (i.e. assuming that half the GCLF is sampled). If we estimate the number of

GCs for MATLAS-2019 in the same way as Lim et al. (2018) we get 12 GCs within $1.5 r_{eff}$ and brighter than the peak of the GCLF, i.e. a total number of 48 GCs and a specific frequency of 111 for MATLAS-2019.

In Fig. 10 we directly compare the Lim et al. (2018) sample with our estimation of MATLAS-2019 adopted for their method. MATLAS-2019 stands out as the most extreme UDG. However, the assumption that half the GCs of MATLAS-2019 are outside of $1.5 r_{eff}$ is not valid, as we demonstrated in Fig. 8. While e.g. Amorisco et al. (2018) found that the majority of the Coma dwarfs have $R_{GC}/R_{eff} \approx 2$ (i.e., the GC system is twice as extended as the stellar light component of the galaxy), we find $R_{GC}/R_{eff} = 0.7$. This does not mean that in general this correction is wrong, but for our particular case of MATLAS-2019 it is not appropriate, which is in line with Amorisco et al. (2018) finding that 4 out of their 55 dwarf galaxies have $R_{GC}/R_{eff} < 1$. For the dwarf galaxies in the Fornax cluster (Prole et al. 2019), the approach to estimate the number of GCs is similar to ours, employing Bayesian consideration by taking the background contamination into account. Therefore, the selection function should be comparable.

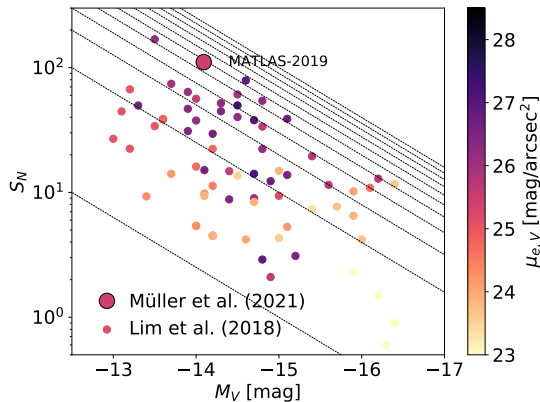


Figure 10. The specific frequency of the Coma cluster dwarfs (Lim et al. 2018) and the UDG MATLAS-2019 (this work). The specific frequency of MATLAS-2019 in this plot is estimated with the same corrections as applied in Lim et al. (2018) to make a direct comparison possible. The color bar indicates the effective surface brightness of the galaxies. The dashed lines correspond to specific frequencies with a constant number of GCs, starting with one GC and then steps of 10 GCs, until 100 GCs is reached.

Other well studied UDGs with a high specific frequency are VCC 1287, NGC 1052-DF2, and DF44. Compared to those, MATLAS-2019 has the highest number of GCs and the highest specific frequency. With the low uncertainty of our measurement we can claim that MATLAS-2019 is extraordinary when it comes to

the abundance of GCs and possibly represents an upper limit of the number of GCs in UDGs – at least within our current knowledge. MATLAS-2019 was initially selected for follow-up studies as having the highest number of GC candidates in the MATLAS survey. This in principle suggests that we should not expect many UDGs in that sample having a higher abundance of GCs. The fact that MATLAS-2019 has such a high abundance is thus not very surprising. It also suggests that UDGs of the failed Milky Way type may be rare (at least based on environments probed by MATLAS), as we would expect them to harbour about 100 GCs or more (van Dokkum et al. 2016).

5. THE DARK MATTER MASS

The number of GCs in a system offers a means to estimate the virial mass of UDGs (Beasley et al. 2016). The virial mass of a galaxy scales linearly with the number of GCs over 6 orders of magnitude (Harris et al. 2013; Burkert & Forbes 2020), the relation only flattens for halos smaller than $10^{10} M_{\odot}$. According to Harris et al. (2017), the virial mass M_{halo} of a galaxy is connected to the total mass of the GC system M_{GC} with:

$$M_{GC}/M_{halo} = 2.9 \times 10^{-5} \quad (10)$$

Assuming a mean mass of a GC to be $1 \times 10^5 M_{\odot}$ for dwarf galaxies (Harris et al. 2017), this yields a GC system mass of $M_{GC} = 2.6 \pm 0.6 \times 10^6 M_{\odot}$ and a halo mass of $M_{halo} = 9 \pm 2 \times 10^{10} M_{\odot}$ for MATLAS-2019. This is above the expected range of bright dwarf galaxies ($M_{halo} = [1.5, 5.0] \times 10^{10} M_{\odot}$, Behroozi et al. 2013; Read et al. 2017; Bullock & Boylan-Kolchin 2017) but also below the mass of the LMC with $2.5 \times 10^{11} M_{\odot}$ (Peñarrubia et al. 2016; Erkal & Belokurov 2020) by a factor of three, i.e. it’s somewhere between the brightest dwarfs and LMC-like galaxies. With an absolute magnitude of -14.1 ± 0.2 mag in the V band⁴, this gives a mass-to-light ratio of $M_{halo}/L_V = 1260_{-555}^{+868} M_{\odot}/L_{\odot}$. The high number of GCs suggests a rather massive halo of dark matter for the galaxy’s stellar mass, but not that of a failed Milky Way – in comparison, the Milky Way is more than ten times more massive with a virial mass of $1.3 \pm 0.3 \times 10^{12} M_{\odot}$ estimated through its GCs (Posti & Helmi 2019).

⁴ The apparent magnitude provided in Müller et al. (2020) was off due to an error in the photometric calibration of the zero point. This explains the discrepancy in the photometry between Müller et al. (2020) and Forbes et al. (2021). The correct apparent V band magnitude measured on the MATLAS data is 17.44 mag, which is consistent with the value of 17.48 mag from Forbes et al. (2021).

Finally, we present all relevant properties of MATLAS-2019 in Table 2.

Table 2. The photometric and the derived properties of MATLAS-2019.

	MATLAS-2019	Reference
RA (J2000.0)	15:05:20.34	(1)
Dec (J2000.0)	+01:48:44.9	(1)
m_V (mag)	17.44	(2)
$\mu_{eff,V}$ (mag/arcsec ²)	25.6	(2)
r_{eff} (arcsec)	17.2	(2)
Sérsic n	0.73	(2)
$g - r$ (mag)	0.59	(2)
$g - i$ (mag)	0.85	(2)
ellipticity e	0.10	(2)
v_{sys}	2156.0±9.4	(3)
D (Mpc)	20.7 ^{+2.3} _{-2.1}	(1)
M_V (mag)	-14.1±0.2	(1)
r_{eff} (kpc)	1.7±0.2	(1)
σ_{GCs} (km/s)	9.4 ^{+7.0} _{-5.4}	(3)
$\sigma_{stellar}$ (km/s)	17±2	(4)
[Fe/H]	-1.33 ^{+0.19} _{-0.01}	(3)
age	11.2 ^{+1.8} _{-0.8}	(3)
N_{GC}	26±6	(1)
S_N	58±14	(1)
M_{halo}/L_V (M_\odot/L_\odot)	1260 ⁺⁸⁶⁸ ₋₅₅₅	(1)

NOTE—The references are: (1) this work; (2) Poulain et al. (2021); (3) (Müller et al. 2020); and (4) (Forbes et al. 2021).

6. DISCUSSION AND CONCLUSIONS

The discovery of the ultra-diffuse galaxy MATLAS-2019 in the MATLAS deep imaging survey was followed-up with MUSE spectroscopy. While the metallicity and age estimation of the stellar body is consistent with that of other dwarf galaxies, the number of luminous GCs seemed to be too high and the measured velocity dispersion suggested a low dark matter content within this galaxy. To assess these two issues, we have observed MATLAS-2019 with the HST using two band imaging. These observations revealed a large population of 26±6 GC candidates associated with MATLAS-2019 with V band magnitudes that follow a normal distribution, as expected from a well-populated GCLF. This would solve the question about the luminous GCs – they are simply the bright end of the GCLF. We derive a specific frequency of $S_N = 58 \pm 14$, which is at the high end of the measurements of other dwarf galaxies and may

therefore be one of the UDGs with the largest number of GCs. This is expected, since MATLAS-2019 was selected for follow-up observations because it had the highest number of possible GCs based on ground-based observations of over 2000 dwarf galaxies in the MATLAS survey. This, however, also suggests that failed Milky Way type galaxies, which were proposed as one of the origins for UDGs, may be relatively rare in the environments we have probed with MATLAS, because we would expect them to have over 100 GCs. If the UDG with the highest number of potential GCs in the MATLAS survey has only a fraction of the number of GCs to be considered a failed Milky Way type galaxy, it is unlikely that other UDGs in this survey are of this type.

Because the GCs are partially resolved with the superior image quality of space-based telescopes like the HST, we were able to measure their sizes. All GCs are consistent with the sizes expected from the GCs of the Local Group.

What can we learn about the history of MATLAS-2019 from the abundance of GCs? This low-surface brightness galaxy must have had high-density star formation and a high star formation rate to form such massive GCs as we observe today. And while much of the mass was locked up in GCs, the remaining stars must have spread out to form such a diffuse galaxy. Carleton et al. (2021) suggested based on simulations of cluster UDGs that they may have an excess of GCs due a combination of a) a higher star formation rate density at high redshift, when most of their star formation occurred, and b) earlier cluster infall times, shutting down the star formation. Because they would fall in earlier, they will experience more tidal effects enlarging the galaxies. While MATLAS-2019 is not in a cluster, the NGC 5846 group of galaxies is a dense galactic environment, so this model may provide an avenue to understand the formation history of MATLAS-2019.

The number of GCs correlates linearly with the virial mass of a galaxy. This idea has its origins in the formation of galaxies through minor mergers: the more mergers a halo experienced, the more mass and the more GCs it accreted. Following such a trend, MATLAS-2019 with its 26 most likely GC candidates would host a vastly dark matter dominated halo with a mass-to-light ratio of over 1000. This provides grounds to state that MATLAS-2019 is not lacking dark matter, on the contrary, it possesses a massive dark matter halo compared to other dwarf galaxies.

ACKNOWLEDGMENTS

We thank the referee – Mario Mateo – for his excellent referee report, which greatly helped to improve this manuscript. Based on observations with the NASA/ESA Hubble Space Telescope obtained [from the Data Archive] at the Space Telescope Science Institute, which is operated by the Association of Universities for Research in Astronomy, Incorporated, under NASA contract NAS5- 26555. Support for Program number (GO-16082) was provided through a grant from the STScI under NASA contract NAS5- 26555. O.M. is grateful to the Swiss National Science Foundation for financial support. PRD gratefully acknowledges support from grant HST-GO-16082.002-A M.P. acknowledges the Vice Rector for Research of the University of Innsbruck for the granted scholarship. S.P. acknowledges support from the New Researcher Program (No. 2019R1C1C1009600) through the National Research Foundation of Korea. This research made use of photutils, an Astropy package for detection and photometry of astronomical sources (Bradley et al. 2020).

Facilities: HST(STIS)

Software: emcee (Foreman-Mackey et al. 2013), GALFIT (Peng et al. 2002), sep (Barbary 2016), photutils (Bradley et al. 2020), astropy (Astropy Collaboration et al. 2013), Source Extractor (Bertin & Arnouts 1996)

REFERENCES

- Amorisco, N. C., Monachesi, A., Agnello, A., & White, S. D. M. 2018, *MNRAS*, 475, 4235, doi: [10.1093/mnras/sty116](https://doi.org/10.1093/mnras/sty116)
- Astropy Collaboration, Robitaille, T. P., Tollerud, E. J., et al. 2013, *A&A*, 558, A33, doi: [10.1051/0004-6361/201322068](https://doi.org/10.1051/0004-6361/201322068)
- Barbary, K. 2016, *The Journal of Open Source Software*, 1, 58, doi: [10.21105/joss.00058](https://doi.org/10.21105/joss.00058)
- Beasley, M. A., Romanowsky, A. J., Pota, V., et al. 2016, *ApJL*, 819, L20, doi: [10.3847/2041-8205/819/2/L20](https://doi.org/10.3847/2041-8205/819/2/L20)
- Behroozi, P. S., Marchesini, D., Wechsler, R. H., et al. 2013, *ApJL*, 777, L10, doi: [10.1088/2041-8205/777/1/L10](https://doi.org/10.1088/2041-8205/777/1/L10)
- Bertin, E., & Arnouts, S. 1996, *A&AS*, 117, 393, doi: [10.1051/aas:1996164](https://doi.org/10.1051/aas:1996164)
- Bilek, M., Müller, O., & Famaey, B. 2019, *A&A*, 627, L1, doi: [10.1051/0004-6361/201935840](https://doi.org/10.1051/0004-6361/201935840)
- Bilek, M., Duc, P.-A., Cuillandre, J.-C., et al. 2020, *MNRAS*, 498, 2138, doi: [10.1093/mnras/staa2248](https://doi.org/10.1093/mnras/staa2248)
- Binggeli, B., Sandage, A., & Tammann, G. A. 1985, *AJ*, 90, 1681, doi: [10.1086/113874](https://doi.org/10.1086/113874)
- Binggeli, B., Tarengi, M., & Sandage, A. 1990, *A&A*, 228, 42
- Blakeslee, J. P., Tonry, J. L., & Metzger, M. R. 1997, *AJ*, 114, 482, doi: [10.1086/118488](https://doi.org/10.1086/118488)
- Bogdan, A. 2020, arXiv e-prints, arXiv:2009.07846, <https://arxiv.org/abs/2009.07846>
- Bradley, L., Sipőcz, B., Robitaille, T., et al. 2020, *astropy/photutils: 1.0.0*, 1.0.0, Zenodo, doi: [10.5281/zenodo.4044744](https://doi.org/10.5281/zenodo.4044744)
- Bullock, J. S., & Boylan-Kolchin, M. 2017, *ARA&A*, 55, 343, doi: [10.1146/annurev-astro-091916-055313](https://doi.org/10.1146/annurev-astro-091916-055313)
- Burkert, A., & Forbes, D. A. 2020, *AJ*, 159, 56, doi: [10.3847/1538-3881/ab5b0e](https://doi.org/10.3847/1538-3881/ab5b0e)
- Cappellari, M., Emsellem, E., Krajnović, D., et al. 2011, *MNRAS*, 413, 813, doi: [10.1111/j.1365-2966.2010.18174.x](https://doi.org/10.1111/j.1365-2966.2010.18174.x)
- Carleton, T., Guo, Y., Munshi, F., Tremmel, M., & Wright, A. 2021, *MNRAS*, doi: [10.1093/mnras/stab031](https://doi.org/10.1093/mnras/stab031)
- Carlsten, S. G., Greco, J. P., Beaton, R. L., & Greene, J. E. 2020, *ApJ*, 891, 144, doi: [10.3847/1538-4357/ab7758](https://doi.org/10.3847/1538-4357/ab7758)
- Chiboucas, K., Karachentsev, I. D., & Tully, R. B. 2009, *AJ*, 137, 3009, doi: [10.1088/0004-6256/137/2/3009](https://doi.org/10.1088/0004-6256/137/2/3009)
- Chilingarian, I. V., Afanasiev, A. V., Grishin, K. A., Fabricant, D., & Moran, S. 2019, *ApJ*, 884, 79, doi: [10.3847/1538-4357/ab4205](https://doi.org/10.3847/1538-4357/ab4205)
- Collins, M. L. M., Tollerud, E. J., Rich, R. M., et al. 2020, *MNRAS*, 491, 3496, doi: [10.1093/mnras/stz3252](https://doi.org/10.1093/mnras/stz3252)
- Conselice, C. J., Gallagher, John S., I., & Wyse, R. F. G. 2003, *AJ*, 125, 66, doi: [10.1086/345385](https://doi.org/10.1086/345385)

- Crnojević, D., Sand, D. J., Caldwell, N., et al. 2014, *ApJL*, 795, L35, doi: [10.1088/2041-8205/795/2/L35](https://doi.org/10.1088/2041-8205/795/2/L35)
- Dalcanton, J. J., Spergel, D. N., Gunn, J. E., Schmidt, M., & Schneider, D. P. 1997, *AJ*, 114, 635, doi: [10.1086/118499](https://doi.org/10.1086/118499)
- Danieli, S., van Dokkum, P., & Conroy, C. 2018, *ApJ*, 856, 69, doi: [10.3847/1538-4357/aaadfb](https://doi.org/10.3847/1538-4357/aaadfb)
- Danieli, S., van Dokkum, P., Conroy, C., Abraham, R., & Romanowsky, A. J. 2019, *ApJL*, 874, L12, doi: [10.3847/2041-8213/ab0e8c](https://doi.org/10.3847/2041-8213/ab0e8c)
- de Rijcke, S., Penny, S. J., Conselice, C. J., Valcke, S., & Held, E. V. 2009, *MNRAS*, 393, 798, doi: [10.1111/j.1365-2966.2008.14229.x](https://doi.org/10.1111/j.1365-2966.2008.14229.x)
- Duc, P.-A. 2020, arXiv e-prints, arXiv:2007.13874. <https://arxiv.org/abs/2007.13874>
- Duc, P.-A., Cuillandre, J.-C., Karabal, E., et al. 2015, *MNRAS*, 446, 120, doi: [10.1093/mnras/stu2019](https://doi.org/10.1093/mnras/stu2019)
- Egenthaler, P., & Zeilinger, W. W. 2010, *A&A*, 511, A12, doi: [10.1051/0004-6361/200811013](https://doi.org/10.1051/0004-6361/200811013)
- Emsellem, E., van der Burg, R. F. J., Fensch, J., et al. 2019, *A&A*, 625, A76, doi: [10.1051/0004-6361/201834909](https://doi.org/10.1051/0004-6361/201834909)
- Erkal, D., & Belokurov, V. A. 2020, *MNRAS*, 495, 2554, doi: [10.1093/mnras/staa1238](https://doi.org/10.1093/mnras/staa1238)
- Fahrion, K., Georgiev, I., Hilker, M., et al. 2019, *A&A*, 625, A50, doi: [10.1051/0004-6361/201834941](https://doi.org/10.1051/0004-6361/201834941)
- Ferguson, H. C., & Binggeli, B. 1994, *AAPR*, 6, 67, doi: [10.1007/BF01208252](https://doi.org/10.1007/BF01208252)
- Forbes, D. A., Gannon, J., Couch, W. J., et al. 2019, *A&A*, 626, A66, doi: [10.1051/0004-6361/201935499](https://doi.org/10.1051/0004-6361/201935499)
- Forbes, D. A., Gannon, J. S., Romanowsky, A. J., et al. 2021, *MNRAS*, 500, 1279, doi: [10.1093/mnras/staa3289](https://doi.org/10.1093/mnras/staa3289)
- Foreman-Mackey, D., Hogg, D. W., Lang, D., & Goodman, J. 2013, *PASP*, 125, 306, doi: [10.1086/670067](https://doi.org/10.1086/670067)
- Gannon, J. S., Forbes, D. A., Romanowsky, A. J., et al. 2020, *MNRAS*, 495, 2582, doi: [10.1093/mnras/staa1282](https://doi.org/10.1093/mnras/staa1282)
- Georgiev, I. Y., Puzia, T. H., Goudfrooij, P., & Hilker, M. 2010, *MNRAS*, 406, 1967, doi: [10.1111/j.1365-2966.2010.16802.x](https://doi.org/10.1111/j.1365-2966.2010.16802.x)
- Goodman, J., & Weare, J. 2010, *Communications in Applied Mathematics and Computational Science*, 5, 65, doi: [10.2140/camcos.2010.5.65](https://doi.org/10.2140/camcos.2010.5.65)
- Habas, R., Marleau, F. R., Duc, P.-A., et al. 2020, *MNRAS*, 491, 1901, doi: [10.1093/mnras/stz3045](https://doi.org/10.1093/mnras/stz3045)
- Harris, W. E. 2010, arXiv e-prints, arXiv:1012.3224. <https://arxiv.org/abs/1012.3224>
- . 2018, *AJ*, 156, 296, doi: [10.3847/1538-3881/aaedb8](https://doi.org/10.3847/1538-3881/aaedb8)
- Harris, W. E., Blakeslee, J. P., & Harris, G. L. H. 2017, *ApJ*, 836, 67, doi: [10.3847/1538-4357/836/1/67](https://doi.org/10.3847/1538-4357/836/1/67)
- Harris, W. E., Harris, G. L. H., & Alessi, M. 2013, *ApJ*, 772, 82, doi: [10.1088/0004-637X/772/2/82](https://doi.org/10.1088/0004-637X/772/2/82)
- Harris, W. E., Harris, G. L. H., Holland, S. T., & McLaughlin, D. E. 2002, *AJ*, 124, 1435, doi: [10.1086/342017](https://doi.org/10.1086/342017)
- Harris, W. E., & van den Bergh, S. 1981, *AJ*, 86, 1627, doi: [10.1086/113047](https://doi.org/10.1086/113047)
- Hilker, M., Infante, L., Vieira, G., Kissler-Patig, M., & Richtler, T. 1999, *A&AS*, 134, 75, doi: [10.1051/aas:1999434](https://doi.org/10.1051/aas:1999434)
- Hudson, M. J., Harris, G. L., & Harris, W. E. 2014, *ApJL*, 787, L5, doi: [10.1088/2041-8205/787/1/L5](https://doi.org/10.1088/2041-8205/787/1/L5)
- Huxor, A. P., Mackey, A. D., Ferguson, A. M. N., et al. 2014, *MNRAS*, 442, 2165, doi: [10.1093/mnras/stu771](https://doi.org/10.1093/mnras/stu771)
- Iodice, E., Cantiello, M., Hilker, M., et al. 2020, *A&A*, 642, A48, doi: [10.1051/0004-6361/202038523](https://doi.org/10.1051/0004-6361/202038523)
- Javanmardi, B., Martinez-Delgado, D., Kroupa, P., et al. 2016, *A&A*, 588, A89, doi: [10.1051/0004-6361/201527745](https://doi.org/10.1051/0004-6361/201527745)
- Karachentsev, I. D., Karachentseva, V. E., Suchkov, A. A., & Grebel, E. K. 2000, *A&AS*, 145, 415, doi: [10.1051/aas:2000249](https://doi.org/10.1051/aas:2000249)
- Kim, D., & Jerjen, H. 2015, *ApJL*, 808, L39, doi: [10.1088/2041-8205/808/2/L39](https://doi.org/10.1088/2041-8205/808/2/L39)
- Koda, J., Yagi, M., Yamanoi, H., & Komiyama, Y. 2015, *ApJL*, 807, L2, doi: [10.1088/2041-8205/807/1/L2](https://doi.org/10.1088/2041-8205/807/1/L2)
- Kovács, O. E., Bogdán, Á., & Canning, R. E. A. 2019, *ApJL*, 879, L12, doi: [10.3847/2041-8213/ab2916](https://doi.org/10.3847/2041-8213/ab2916)
- Laporte, C. F. P., Agnello, A., & Navarro, J. F. 2019, *MNRAS*, 484, 245, doi: [10.1093/mnras/sty2891](https://doi.org/10.1093/mnras/sty2891)
- Lim, S., Peng, E. W., Côté, P., et al. 2018, *ApJ*, 862, 82, doi: [10.3847/1538-4357/aacb81](https://doi.org/10.3847/1538-4357/aacb81)
- Lim, S., Côté, P., Peng, E. W., et al. 2020, *ApJ*, 899, 69, doi: [10.3847/1538-4357/aba433](https://doi.org/10.3847/1538-4357/aba433)
- Liu, C., Peng, E. W., Côté, P., et al. 2015, *ApJ*, 812, 34, doi: [10.1088/0004-637X/812/1/34](https://doi.org/10.1088/0004-637X/812/1/34)
- Liu, C., Côté, P., Peng, E. W., et al. 2020, *ApJS*, 250, 17, doi: [10.3847/1538-4365/abad91](https://doi.org/10.3847/1538-4365/abad91)
- Mahdavi, A., Trentham, N., & Tully, R. B. 2005, *AJ*, 130, 1502, doi: [10.1086/444560](https://doi.org/10.1086/444560)
- Majewski, S. R., Patterson, R. J., Dinescu, D. I., et al. 2000, in *Liege International Astrophysical Colloquia*, Vol. 35, *Liege International Astrophysical Colloquia*, ed. A. Noels, P. Magain, D. Caro, E. Jehin, G. Parmentier, & A. A. Thoul, 619. <https://arxiv.org/abs/astro-ph/9910278>
- Makarov, D. I., Makarova, L. N., Pustilnik, S. A., & Borisov, S. B. 2017, *MNRAS*, 466, 556, doi: [10.1093/mnras/stw3145](https://doi.org/10.1093/mnras/stw3145)
- Mancera Piña, P. E., Fraternali, F., Adams, E. A. K., et al. 2019, *ApJL*, 883, L33, doi: [10.3847/2041-8213/ab40c7](https://doi.org/10.3847/2041-8213/ab40c7)
- Martin, N. F., Collins, M. L. M., Longeard, N., & Tollerud, E. 2018, *ApJL*, 859, L5, doi: [10.3847/2041-8213/aac216](https://doi.org/10.3847/2041-8213/aac216)

- Martínez-Delgado, D., Läsker, R., Sharina, M., et al. 2016, *AJ*, 151, 96, doi: [10.3847/0004-6256/151/4/96](https://doi.org/10.3847/0004-6256/151/4/96)
- McGaugh, S. S., & Bothun, G. D. 1994, *AJ*, 107, 530, doi: [10.1086/116874](https://doi.org/10.1086/116874)
- McGaugh, S. S., & Wolf, J. 2010, *ApJ*, 722, 248, doi: [10.1088/0004-637X/722/1/248](https://doi.org/10.1088/0004-637X/722/1/248)
- Mihos, J. C., Harding, P., Feldmeier, J. J., et al. 2017, *ApJ*, 834, 16, doi: [10.3847/1538-4357/834/1/16](https://doi.org/10.3847/1538-4357/834/1/16)
- Mihos, J. C., Durrell, P. R., Ferrarese, L., et al. 2015, *ApJL*, 809, L21, doi: [10.1088/2041-8205/809/2/L21](https://doi.org/10.1088/2041-8205/809/2/L21)
- Müller, O., & Jerjen, H. 2020, *A&A*, 644, A91, doi: [10.1051/0004-6361/202038862](https://doi.org/10.1051/0004-6361/202038862)
- Müller, O., Jerjen, H., & Binggeli, B. 2015, *A&A*, 583, A79, doi: [10.1051/0004-6361/201526748](https://doi.org/10.1051/0004-6361/201526748)
- . 2017, *A&A*, 597, A7, doi: [10.1051/0004-6361/201628921](https://doi.org/10.1051/0004-6361/201628921)
- . 2018, *A&A*, 615, A105, doi: [10.1051/0004-6361/201832897](https://doi.org/10.1051/0004-6361/201832897)
- Müller, O., Marleau, F. R., Duc, P.-A., et al. 2020, *A&A*, 640, A106, doi: [10.1051/0004-6361/202038351](https://doi.org/10.1051/0004-6361/202038351)
- Müller, O., Fahrion, K., Rejkuba, M., et al. 2021, *A&A*, 645, A92, doi: [10.1051/0004-6361/202039359](https://doi.org/10.1051/0004-6361/202039359)
- Ogiya, G. 2018, *MNRAS*, 480, L106, doi: [10.1093/mnrasl/sly138](https://doi.org/10.1093/mnrasl/sly138)
- Park, H. S., Moon, D.-S., Zaritsky, D., et al. 2017, *ApJ*, 848, 19, doi: [10.3847/1538-4357/aa88ab](https://doi.org/10.3847/1538-4357/aa88ab)
- Peñarrubia, J., Gómez, F. A., Besla, G., Erkal, D., & Ma, Y.-Z. 2016, *MNRAS*, 456, L54, doi: [10.1093/mnrasl/slv160](https://doi.org/10.1093/mnrasl/slv160)
- Peacock, M. B., Maccarone, T. J., Knigge, C., et al. 2010, *MNRAS*, 402, 803, doi: [10.1111/j.1365-2966.2009.15952.x](https://doi.org/10.1111/j.1365-2966.2009.15952.x)
- Peng, C. Y., Ho, L. C., Impey, C. D., & Rix, H.-W. 2002, *AJ*, 124, 266, doi: [10.1086/340952](https://doi.org/10.1086/340952)
- Peng, E. W., & Lim, S. 2016, *ApJL*, 822, L31, doi: [10.3847/2041-8205/822/2/L31](https://doi.org/10.3847/2041-8205/822/2/L31)
- Penny, S. J., Forbes, D. A., Pimblet, K. A., & Floyd, D. J. E. 2014, *MNRAS*, 443, 3381, doi: [10.1093/mnras/stu1397](https://doi.org/10.1093/mnras/stu1397)
- Posti, L., & Helmi, A. 2019, *A&A*, 621, A56, doi: [10.1051/0004-6361/201833355](https://doi.org/10.1051/0004-6361/201833355)
- Poulain, M., Marleau, F. R., Habas, R., et al. 2021, *MNRAS*, 506, 5494, doi: [10.1093/mnras/stab2092](https://doi.org/10.1093/mnras/stab2092)
- Prole, D. J., Hilker, M., van der Burg, R. F. J., et al. 2019, *MNRAS*, 484, 4865, doi: [10.1093/mnras/stz326](https://doi.org/10.1093/mnras/stz326)
- Read, J. I., Iorio, G., Agertz, O., & Fraternali, F. 2017, *MNRAS*, 467, 2019, doi: [10.1093/mnras/stx147](https://doi.org/10.1093/mnras/stx147)
- Rejkuba, M. 2012, *Ap&SS*, 341, 195, doi: [10.1007/s10509-012-0986-9](https://doi.org/10.1007/s10509-012-0986-9)
- Rekola, R., Jerjen, H., & Flynn, C. 2005, *A&A*, 437, 823, doi: [10.1051/0004-6361:20042198](https://doi.org/10.1051/0004-6361:20042198)
- Saifollahi, T., Trujillo, I., Beasley, M. A., Peletier, R. F., & Knapen, J. H. 2020, arXiv e-prints, arXiv:2006.14630, <https://arxiv.org/abs/2006.14630>
- Sandage, A., & Binggeli, B. 1984, *AJ*, 89, 919, doi: [10.1086/113588](https://doi.org/10.1086/113588)
- Schlafly, E. F., & Finkbeiner, D. P. 2011, *ApJ*, 737, 103, doi: [10.1088/0004-637X/737/2/103](https://doi.org/10.1088/0004-637X/737/2/103)
- Spitler, L. R., & Forbes, D. A. 2009, *MNRAS*, 392, L1, doi: [10.1111/j.1745-3933.2008.00567.x](https://doi.org/10.1111/j.1745-3933.2008.00567.x)
- Toloba, E., Lim, S., Peng, E., et al. 2018, *ApJL*, 856, L31, doi: [10.3847/2041-8213/aab603](https://doi.org/10.3847/2041-8213/aab603)
- Torrealba, G., Koposov, S. E., Belokurov, V., & Irwin, M. 2016, *MNRAS*, 459, 2370, doi: [10.1093/mnras/stw733](https://doi.org/10.1093/mnras/stw733)
- van der Burg, R. F. J., Hoekstra, H., Muzzin, A., et al. 2017, *A&A*, 607, A79, doi: [10.1051/0004-6361/201731335](https://doi.org/10.1051/0004-6361/201731335)
- van Dokkum, P., Danieli, S., Abraham, R., Conroy, C., & Romanowsky, A. J. 2019a, *ApJL*, 874, L5, doi: [10.3847/2041-8213/ab0d92](https://doi.org/10.3847/2041-8213/ab0d92)
- van Dokkum, P., Abraham, R., Brodie, J., et al. 2016, *ApJL*, 828, L6, doi: [10.3847/2041-8205/828/1/L6](https://doi.org/10.3847/2041-8205/828/1/L6)
- van Dokkum, P., Abraham, R., Romanowsky, A. J., et al. 2017, *ApJL*, 844, L11, doi: [10.3847/2041-8213/aa7ca2](https://doi.org/10.3847/2041-8213/aa7ca2)
- van Dokkum, P., Danieli, S., Cohen, Y., et al. 2018a, *Nature*, 555, 629, doi: [10.1038/nature25767](https://doi.org/10.1038/nature25767)
- van Dokkum, P., Cohen, Y., Danieli, S., et al. 2018b, *ApJL*, 856, L30, doi: [10.3847/2041-8213/aab60b](https://doi.org/10.3847/2041-8213/aab60b)
- van Dokkum, P., Wasserman, A., Danieli, S., et al. 2019b, *ApJ*, 880, 91, doi: [10.3847/1538-4357/ab2914](https://doi.org/10.3847/1538-4357/ab2914)
- van Dokkum, P. G., Abraham, R., Merritt, A., et al. 2015, *ApJL*, 798, L45, doi: [10.1088/2041-8205/798/2/L45](https://doi.org/10.1088/2041-8205/798/2/L45)
- Venhola, A., Peletier, R., Laurikainen, E., et al. 2017, *A&A*, 608, A142, doi: [10.1051/0004-6361/201730696](https://doi.org/10.1051/0004-6361/201730696)
- Voggel, K., Hilker, M., Baumgardt, H., et al. 2016, *MNRAS*, 460, 3384, doi: [10.1093/mnras/stw1132](https://doi.org/10.1093/mnras/stw1132)
- Walker, M. G., Mateo, M., Olszewski, E. W., et al. 2007, *ApJL*, 667, L53, doi: [10.1086/521998](https://doi.org/10.1086/521998)
- Zaritsky, D., Donnerstein, R., Dey, A., et al. 2019, *ApJS*, 240, 1, doi: [10.3847/1538-4365/aaefe9](https://doi.org/10.3847/1538-4365/aaefe9)

Table 3. All detected GC-like sources within 1.75 effective radius of MATLAS-2019, of which we estimate that 37 are real GC associated with MATLAS-2019. For the calculation of r_h in parsec we used a distance modulus of 31.56 derived from the peak of the GCLF. The asterisks denotes whether the GC was listed in Müller et al. (2020). The magnitudes are extinction corrected. The errors for the absolute V band magnitudes are a combination of the photometric error and the uncertainty in the distance modulus, which dominates the error.

#	RA (J2000.0)	Dec (J2000.0)	F606W (mag)	F606W - F814W (mag)	M_V (mag)	r_h (arcsec)	r_h (pc)	r_c (arcsec)	r_t (arcsec)	d_{center} (arcsec)
1	226.328690	1.811024	24.557±0.041	0.739±0.050	-6.87±0.47	0.058±0.004	5.8±0.3	0.025±0.004	0.438±0.086	22.5
2	226.329288	1.816956	25.800±0.142	0.686±0.196	-5.63±0.49	0.291±0.032	29.0±3.1	0.148±0.019	1.093±0.311	25.5
3	226.329752	1.811939	25.147±0.073	0.675±0.107	-6.28±0.48	0.082±0.011	8.2±1.1	0.019±0.004	1.111±0.584	18.1
4*	226.329915	1.811463	23.674±0.017	0.699±0.024	-7.75±0.47	0.038±0.002	3.8±0.2	0.003±0.001	2.209±0.925	17.8
5	226.330024	1.814198	24.089±0.023	0.717±0.029	-7.34±0.47	0.021±0.003	2.1±0.2	0.008±0.003	0.275±0.058	18.1
6	226.330036	1.810074	24.123±0.019	0.669±0.030	-7.30±0.47	0.045±0.003	4.5±0.2	0.014±0.003	0.342±0.058	19.1
7	226.330482	1.812385	24.475±0.038	0.678±0.047	-6.95±0.47	0.006±0.900	0.6±89.7	0.009±0.156	0.034±0.385	15.4
8	226.330594	1.812373	24.449±0.036	0.653±0.045	-6.98±0.47	0.004±0.009	0.4±0.8	0.016±0.043	0.088±0.116	15.0
9*	226.331081	1.810577	24.128±0.019	0.650±0.030	-7.30±0.47	0.062±0.004	6.2±0.3	0.015±0.002	0.783±0.140	14.9
10	226.331100	1.813403	24.361±0.033	0.774±0.041	-7.07±0.47	0.035±0.003	3.5±0.3	0.014±0.004	0.305±0.066	13.6
11	226.331323	1.812492	25.081±0.071	0.689±0.107	-6.35±0.48	0.070±0.006	7.0±0.6	0.023±0.005	0.573±0.195	12.4
12*	226.331332	1.815083	23.382±0.009	0.715±0.021	-8.05±0.47	0.042±0.002	4.1±0.1	0.003±0.000	49.999±0.000	15.5
13	226.331693	1.819393	25.653±0.119	0.795±0.166	-5.77±0.48	0.130±0.028	12.9±2.7	0.043±0.013	0.612±0.327	27.3
14	226.331837	1.811076	24.157±0.020	0.703±0.030	-7.27±0.47	0.024±0.002	2.4±0.2	0.013±0.004	0.242±0.051	11.7
15	226.332161	1.810717	25.613±0.117	0.665±0.169	-5.81±0.48	0.056±0.007	5.6±0.7	0.033±0.021	0.240±0.124	11.3
16	226.332456	1.808513	24.655±0.038	0.569±0.067	-6.77±0.47	0.001±0.000	0.0±0.0	0.005±0.248	0.025±0.477	16.5
17	226.332657	1.813898	25.014±0.059	0.586±0.100	-6.41±0.47	0.026±0.005	2.6±0.5	0.015±0.016	0.176±0.112	9.2
18	226.332700	1.809457	25.032±0.062	0.853±0.095	-6.40±0.47	0.056±0.009	5.6±0.8	0.011±0.003	0.732±0.353	13.1
19	226.332765	1.815702	25.654±0.119	0.776±0.166	-5.77±0.48	0.155±0.087	15.5±8.7	0.021±0.006	1.010±0.802	13.7
20	226.332857	1.812632	24.438±0.035	0.684±0.043	-6.99±0.47	0.018±0.003	1.8±0.2	0.008±0.006	0.190±0.080	6.9
21	226.333213	1.817496	25.073±0.070	0.639±0.107	-6.35±0.48	0.024±0.004	2.4±0.4	0.018±0.024	0.148±0.108	18.9
22*	226.333478	1.811035	23.159±0.008	0.663±0.013	-8.27±0.47	0.017±0.001	1.7±0.1	0.004±0.001	0.503±0.052	6.9
23	226.333592	1.815197	25.063±0.068	0.793±0.099	-6.36±0.47	0.031±0.004	3.1±0.4	0.024±0.024	0.156±0.093	10.7
24	226.333624	1.815683	24.758±0.048	0.543±0.082	-6.67±0.47	0.022±0.005	2.2±0.5	0.005±0.003	0.431±0.166	12.3
25*	226.333800	1.810589	23.217±0.016	0.723±0.019	-8.21±0.47	0.013±0.001	1.2±0.0	0.006±0.003	0.151±0.034	7.6
26*	226.333895	1.812363	22.510±0.014	0.688±0.017	-8.92±0.47	0.035±0.001	3.5±0.0	0.003±0.000	2.233±0.328	3.1
27	226.333997	1.810966	25.012±0.059	0.719±0.094	-6.42±0.47	0.042±0.004	4.1±0.4	0.009±0.004	0.568±0.254	6.1
28	226.334056	1.810118	23.834±0.016	0.675±0.024	-7.59±0.47	0.024±0.002	2.4±0.2	0.007±0.002	0.298±0.050	8.8
29*	226.334511	1.812922	22.237±0.003	0.695±0.006	-9.19±0.47	0.060±0.001	6.0±0.1	0.005±0.000	2.748±0.322	1.9
30	226.334833	1.809974	25.643±0.118	0.526±0.180	-5.78±0.48	0.026±0.010	2.6±1.0	0.019±0.040	0.152±0.181	9.0
31	226.335019	1.810862	24.548±0.040	0.711±0.053	-6.88±0.47	0.017±0.004	1.7±0.4	0.019±0.015	0.134±0.059	5.9
32*	226.335134	1.813640	23.105±0.009	0.729±0.018	-8.32±0.47	0.028±0.001	2.8±0.1	0.003±0.001	0.779±0.094	4.4
33	226.335388	1.818917	26.168±0.165	0.807±0.226	-5.26±0.50	0.001±0.422	0.0±42.1	0.006±0.928	0.036±3.564	23.3
34*	226.335522	1.812527	23.761±0.015	0.747±0.020	-7.67±0.47	0.007±0.002	0.7±0.2	0.017±0.018	0.096±0.050	2.7
35	226.335539	1.816354	25.390±0.107	0.822±0.141	-6.04±0.48	0.160±0.021	15.9±2.0	0.058±0.007	1.264±0.512	14.3
36*	226.335632	1.811585	22.953±0.006	0.689±0.011	-8.47±0.47	0.038±0.001	3.8±0.1	0.003±0.000	2.184±0.414	4.5
37*	226.335770	1.813566	23.734±0.015	0.717±0.020	-7.69±0.47	0.001±0.220	0.0±21.9	0.010±0.065	0.048±0.166	5.4
38	226.336036	1.812193	25.473±0.107	0.574±0.158	-5.95±0.48	0.118±0.014	11.8±1.4	0.034±0.006	1.176±0.618	4.7
39*	226.336431	1.815219	23.318±0.009	0.760±0.012	-8.11±0.47	0.013±0.002	1.3±0.2	0.017±0.008	0.117±0.029	11.6
40*	226.336516	1.817465	22.940±0.006	0.688±0.011	-8.49±0.47	0.023±0.001	2.3±0.1	0.003±0.001	0.717±0.076	19.1
41	226.336918	1.811995	25.928±0.147	0.653±0.210	-5.50±0.49	0.210±0.149	20.9±14.9	0.026±0.007	4.631±14.363	7.9
42	226.336924	1.818362	26.095±0.155	0.494±0.223	-5.33±0.49	0.126±0.013	12.5±1.3	0.361±0.918	0.275±0.092	22.6
43	226.337516	1.817296	24.386±0.034	0.616±0.043	-7.04±0.47	0.028±0.003	2.8±0.3	0.005±0.002	0.528±0.142	20.0
44	226.338322	1.818318	24.729±0.045	0.652±0.070	-6.70±0.47	0.049±0.005	4.8±0.5	0.008±0.002	0.721±0.266	24.6
45	226.340142	1.817091	24.735±0.046	0.514±0.081	-6.69±0.47	0.001±0.317	0.0±31.5	0.008±0.269	0.036±0.816	25.5
46	226.340199	1.810136	25.933±0.147	0.767±0.202	-5.49±0.49	0.120±0.014	12.0±1.4	0.054±0.010	1.423±0.990	21.3
47	226.340572	1.809045	24.764±0.049	0.743±0.069	-6.66±0.47	0.075±0.005	7.5±0.5	0.017±0.003	0.772±0.229	24.3
48	226.340587	1.814754	25.803±0.143	0.817±0.188	-5.62±0.49	0.001±0.000	0.0±0.0	0.002±0.000	49.999±0.000	22.5
49	226.341214	1.811742	25.313±0.098	0.713±0.138	-6.12±0.48	0.114±0.008	11.3±0.8	0.043±0.007	0.600±0.173	23.4